Magn Reson Med Sci, Vol. 13, No. 4, pp. 231–238, 2014 doi:10.2463/mrms.2013-0108

MAJOR PAPER

Analysis of Susceptibility-Weighted Images of Cortico-Medullary Junction

Taha M. Mehemed[1], Akira Yamamoto[1]*, Tomohisa Okada[1], Mitsunori Kanagaki[1], Takeshi Sawada[1], Emiko Morimoto[1], Jun C. Takahashi[2], Susumu Miyamoto[2], and Kaori Togashi[1]

[1]*Department of Diagnostic Imaging and Nuclear Medicine, Graduate School of Medicine, Kyoto University 54 Kawahara-cho, Shogoin, Sakyo-ku, Kyoto-shi, Kyoto 606–8507, Japan*
[2]*Department of Neurosurgery, Graduate School of Medicine, Kyoto University*
(Received November 1, 2013; Accepted April 2, 2014; published online August 27, 2014)

Objective: We qualitatively evaluated the differences among susceptibility-weighted (SWI), magnitude (MAG), and high pass filtered phase (PHA) images in depicting interlobar differences in the appearance of the signal of the corticomedullary junction (CMJ). We conducted quantitative evaluation to validate the qualitative results.

Materials and Methods: We obtained SWI images from 25 preoperative brain tumor patients (12 men, 13 women, aged 19 to 82 years, mean, 52 years). Two trained neuroradiologists evaluated MAG, PHA, and SWI images. Qualitative evaluation of the CMJ signal and quantitative calculation of the relative signal ratio (RSR) percentages between the CMJ and deep white matter (WM) were conducted at 3 different slice levels of the brain independently for 4 different lobes (frontal, parietal, temporal, and occipital) and compared among MAG, PHA, and SWI. The extent of the area of the CMJ signal was graded on a 4-point scale (Grade 3, >75%; Grade 2, 50 to 75%; Grade 1, 25 to 50%; Grade 0, <25%). Data were statistically analyzed using a nonparametric Friedman test.

Results: The Kappa coefficients between the qualitative and quantitative grades were 0.002 for MAG, 0.0047 for PHA, and 0.050 for SWI. Qualitatively, on the PHA images and SWI, grades of the occipital lobes were significantly higher than those of the other lobes ($P < 0.005$). Quantitatively, PHA images showed statistically significant interlobar differences in RSR percentage values of the CMJ ($P = 0.025$).

Conclusion: Qualitatively, the appearance of the CMJ differed significantly among the different lobes of the brain on SWI and underlying PHA images but not on MAG images. Quantitatively, only PHA images showed significant interlobar differences in the RSR. PHA images are most sensitive to the CMJ signal contrast due to local paramagnetic iron content.

Keywords: ***corticomedullary junction*, *interlobar difference*, *quantitative analysis*, *susceptibility-weighted imaging***

Introduction

Susceptibility-weighted imaging (SWI) is a relatively new magnetic resonance (MR) imaging sequence that relies on local tissue susceptibility, such as that to deposition of iron and to blood-oxygen-level-dependent (BOLD) effect, to create contrast.[1] With the increased clinical availability of MR imaging scanners with high fields, such as 3 tesla, SWI is a reliable sequence for evaluating hemorrhage,[2] migraine,[3] and fine venous structures,[4] quantifying brain iron content at the basal ganglia,[5–8] and identifying brain calcification.[9] However, though MR imaging studies of brain histological specimens are ongoing, *in vivo* studies using SWI in the CMJ are not so common. Details of brain structures, such as the optic radiation (OR), have also been reported as bands of low signal on SWI.[10] The presence of deoxyhemoglobin in the

*Corresponding author, Phone: +81-75-751-3760, Fax: +81-75-771-9709, E-mail: yakira@kuhp.kyoto-u.ac.jp

venules of the CMJ will affect both MAG and PHA images.[11–13] Effects of myelin and other histological components at the CMJ appear mainly on PHA images,[14] and a recent study reported the disappearance of the CMJ signal on PHA images of demyelinated mice brains.[15] Water-macromolecule exchange has been reported as another cause of contrast on PHA images.[16] A combination of the above-mentioned mechanisms might contribute to the final SWI contrast.

The CMJ is a unique anatomical location in the brain, responsible for the interconnection of cortical and subcortical areas and a part of the neural networks of the brain. Recent reports have shown changes in the appearance of the CMJ in Alzheimer's disease using 7T MR SWI or diffusion tensor imaging.[17,18] Knowing the normal appearance of the CMJ and following such age-related changes might give clues about the pathogenesis of Alzheimer's disease. However, research is ongoing to determine its true value in the diagnosis of Alzheimer's disease.

Our daily use of SWI in brain MR imaging examinations has given us the impression that the appearance of the CMJ differs by lobe. Therefore, hypothesizing a differing appearance of the CMJ signal among the different lobes, we evaluated the appearance of the normal CMJ in the different lobes of the brain using SWI. We also investigated MAG and PHA images.

Materials and Methods

Our local ethics committee approved this retrospective analysis of SWI, MAG, and PHA images acquired from January 2009 to December 2010 and waived the requirement for informed patient consent because of the retrospective nature of the study.

Subjects were 25 preoperative brain tumor patients (12 men, 13 women; aged 19 to 82 years, mean age, 52 ± 19.2 years). None of the subjects had symptoms of dementia or cognitive impairment. We did not include patients with tumor extending to the other hemisphere or with mass effect or whose images were degraded by artifact caused by such factors as head motion.

Data acquisition

SWI and magnetization prepared rapid gradient echo (MPRAGE) images were acquired using a 3T MR imaging scanner (Trio A Tim System, SIEMENS Medical Solutions, Erlangen, Germany). The parameters for SWI in axial acquisition were: repetition time (TR), 28 ms; echo time (TE), 20 ms; flip angle, 15 degrees; acquisition matrix, 320×250; field of vision (FOV), 230×180 mm; pixel spacing, $0.72\,\text{mm} \times 0.72\,\text{mm}$; slice thickness, 1.2 mm; slab thickness, 80 slices; high pass filter kernel size, 96×96; and number of averages, one. We reconstructed MAG, PHA, and SWI images.[1] Sagittal 3D-MPRAGE parameters were: TR, 1900 ms; TE, 2.58 ms; and inversion time (TI), 900 ms with 0.9-mm isotropic resolution. The MPRAGE image volume data were reformatted into the axial plane.

Imaging analysis

Qualitative analysis of lobar CMJ grade

Two trained neuroradiologists independently evaluated SWI, MAG, and PHA images for all 25 subjects using a PC-installed DICOM viewer (Centricity™; GE Healthcare, USA). MPRAGE, SWI, PHA, and MAG images were evaluated simultaneously using a spatial cursor function on the picture archiving and communication system (PACS). The spatial cursor function enabled us to evaluate the precise location of the CMJ on MPRAGE and share the spatial information from the cursor among different images. We evaluated low signal at the CMJ on SWI and MAG images. We evaluated high signal at the CMJ on the PHA images because our MR imaging system is left-handed.[19,20]

We evaluated the signal of the CMJ on the nontumor side at the levels of the genu of the corpus callosum for the frontal and parietal lobes, splenium of the corpus callosum for the occipital lobe, and red nucleus for the temporal lobe.

We used a 4-point scale to grade the extent (length of CMJ signal/total length of gray matter) of the CMJ signal visible in the studied lobe (Grade 3, >75% of CMJ signal visible; Grade 2, 50 to 75% visible; Grade 1, 25 to 50% visible; and Grade 0, <25% visible) (Fig. 1).

When the scores for an image did not agree between the 2 evaluators, final scores were decided by consensus.

Quantitative analysis of CMJ signal

Quantitative analysis was conducted for the same subjects at the same slice location to validate the qualitative results.

We coregistered MPRAGE images to SWI using Siemens *syngo* MultiModality Workplace software, manually drew a linear region of interest (ROI) of 3-mm width following the border between the gray (GM) and white matter (WM) on MPRAGE in each lobe at the same slice level evaluated qualitatively, and overlaid the ROI onto SWI, MAG, and PHA images using ImageJ (National Institutes of Health, USA) ROI manager.[21] We then measured the signal intensity for each voxel along the linear CMJ ROI.

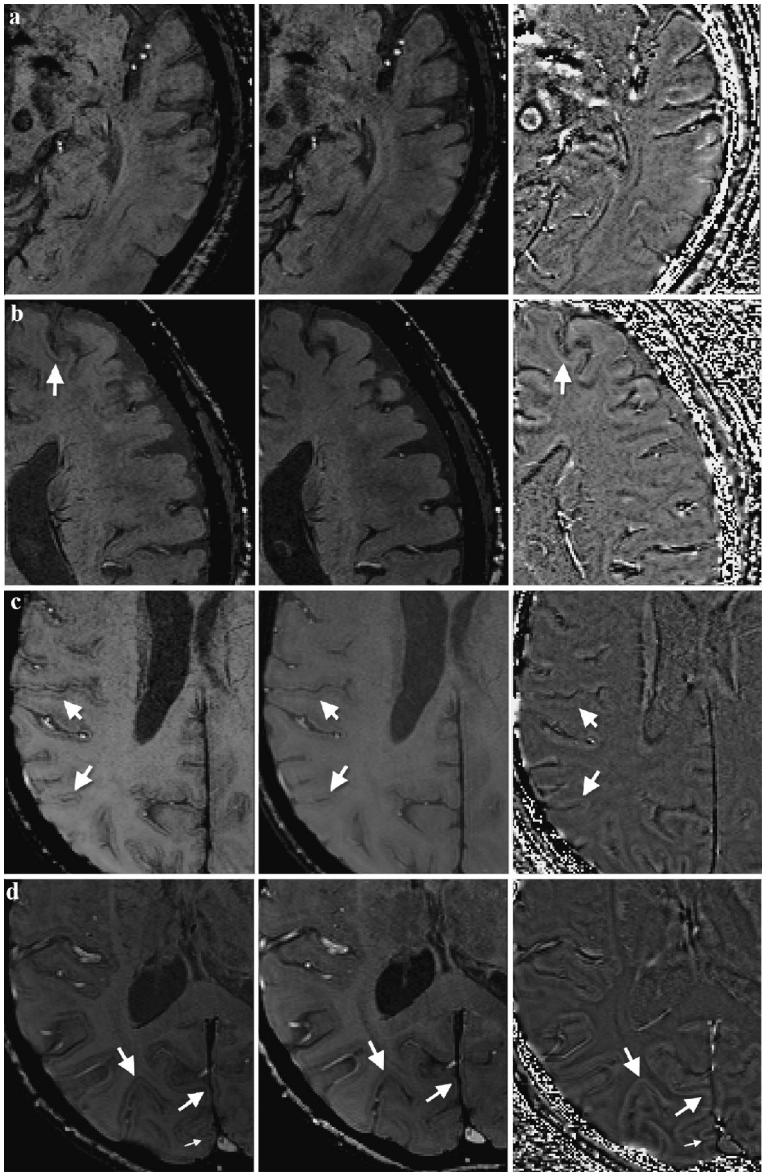

Fig. 1. (**a**) Grade 0 corticomedullary junction (CMJ) signal of temporal lobe on susceptibility-weighted imaging (SWI), corresponding magnitude (MAG) and high pass filtered phase (PHA) images from left to right. (**b**) Grade 1 CMJ signal of frontal lobe on SWI, corresponding MAG and PHA images from left to right. (**c**) Grade 2 CMJ signal of parietal lobe on SWI, corresponding MAG and PHA images from left to right. (**d**) Grade 3 CMJ signal of occipital lobe on SWI, corresponding MAG and PHA images from left to right.

To quantify the signal intensity of the neighboring deep white matter, we used a circular ROI of 10-pixel diameter. We calculated the relative signal ratio (RSR) between the CMJ and neighboring deep WM for every voxel along the linear CMJ ROI in each lobe on all images by dividing the signal intensity value of the CMJ by that of the deep WM: RSR = CMJ/deep WM. For SWI and MAG, we considered all RSR values less than one to represent the CMJ low signal intensity examined qualitatively; for PHA images, we used RSR values greater than one. To determine the percentage of CMJ signal, we counted the total number of voxels with RSR less than one in SWI and MAG images and greater than one in PHA images in each lobe for each patient and then divided that number by the entire number of voxels of the CMJ ROI.

To compare qualitative and quantitative results, we converted the RSR percentages into grades similar to those of the qualitative evaluation.

Statistical analysis

We used the Kappa coefficient to calculate agreement between the scores by independent observations of the 2 evaluators and between the qualita-

tive and quantitative results, logistic regression analysis to evaluate the relationship between age and grade, and a nonparametric Friedman test to analyze the data for interlobar grades for both qualitative and quantitative results. $P < 0.05$ was considered statistically significant after *post hoc* multiple comparisons (Scheffe test).

Results

Qualitative analysis of lobar CMJ grade

No subjects were excluded because of infiltration. The Kappa coefficients of the 2 evaluators, 0.67 for MAG, 0.68 for PHA, and 0.62 for SWI images, demonstrated substantial agreement. There was no significant age-related interlobar difference in CMJ grades.

Table 1 shows the grades after consensus of the CMJ signal on MAG (Table 1a), PHA (Table 1b), and SWI images (Table 1c). The grades were highest at the occipital lobe compared with other lobes, but differed little between MAG and the PHA and SWI images; we observed no significant difference among the grades of the different lobes on the MAG images (Table 2). On the PHA images, grades of the occipital lobe were significantly higher than any of the frontal and temporal lobe grades ($P = 0.001$) but not significant compared with the parietal lobe ($P = 0.10$, Table 2). The occipital lobe showed significantly higher grades on SWI compared with the frontal ($P = 0.001$), temporal ($P = 0.001$), and parietal lobes ($P = 0.015$) (Table 2). Grades of the parietal lobe were significantly higher than those of the temporal lobe on the PHA images ($P = 0.001$) but not the SWI images ($P = 0.42$) and MAG images ($P = 0.80$) (Table 2).

Table 1a. Distribution of qualitative grades among the different lobes on magnitude (MAG) images

	Frontal	Parietal	Occipital	Temporal
Grade 0	16	15	12	19
Grade 1	3	5	9	4
Grade 2	5	5	3	2
Grade 3	1	0	1	0
Total	25	25	25	25

Table 1b. Distribution of qualitative grades among the different lobes on high pass filtered phase (PHA) images

	Frontal	Parietal	Occipital	Temporal
Grade 0	8	9	0	13
Grade 1	9	8	2	11
Grade 2	4	5	11	1
Grade 3	4	3	12	0
Total	25	25	25	25

Table 1c. Distribution of qualitative grades among the different lobes on susceptibility-weighted imaging (SWI)

	Frontal	Parietal	Occipital	Temporal
Grade 0	11	9	2	11
Grade 1	10	9	8	10
Grade 2	4	5	10	4
Grade 3	0	2	5	0
Total	25	25	25	25

Quantitative analysis of CMJ signal

RSR results: Table 3 shows the distribution of CMJ RSR percentage values on MAG (3a), PHA (3b), and SWI (3c). PHA images showed statistically significant interlobar differences in RSR percentage values ($P = 0.025$), with significantly higher RSR percentage values for the occipital lobe than the frontal and parietal lobes ($P < 0.05$ for both) and for the parietal lobe than the frontal lobe ($P < 0.05$) (Table 4). There was no significant age-related interlobar difference of CMJ RSR percentages.

The Kappa coefficients between the qualitative and quantitative grades were 0.002 for MAG, 0.047 for PHA, and 0.050 for SWI. The 2 results showed only slight agreement.

Discussion

In this study, our quantitative results showed significant differences in the appearance of the CMJ among the different lobes of the brain on PHA images, while our qualitative results also showed significant interlobar difference, there was only slight

Table 2. Qualitative interlobar comparison for magnitude (MAG), high pass filtered phase (PHA), and susceptibility-weighted (SWI) images using nonparametric Friedman test

	MAG	PHA	SWI
P value	0.47	<0.001	<0.001
Interlobar comparisons		O vs F ($P < 0.001$)	O vs F ($P < 0.001$)
		O vs T ($P < 0.001$)	O vs T ($P < 0.001$)
		P vs T ($P = 0.001$)	O vs T ($P = 0.015$)

O, occipital lobe; F, frontal lobe; P, parietal lobe; T, temporal lobe

Table 3a. Distribution of quantitative grades among the different lobes on magnitude (MAG) images

	Frontal	Parietal	Occipital	Temporal
Grade 0	6	6	2	7
Grade 1	3	4	6	7
Grade 2	4	7	12	5
Grade 3	12	8	5	6
Total	25	25	25	25

Table 3b. Distribution of quantitative grades among the different lobes on high pass filtered phase (PHA) images

	Frontal	Parietal	Occipital	Temporal
Grade 0	0	0	0	1
Grade 1	7	5	6	7
Grade 2	18	18	17	16
Grade 3	0	2	2	1
Total	25	25	25	25

Table 3c. Distribution of quantitative grades among the different lobes on susceptibility-weighted (SWI) images

	Frontal	Parietal	Occipital	Temporal
Grade 0	4	4	2	5
Grade 1	4	3	5	6
Grade 2	3	6	6	7
Grade 3	14	12	12	7
Total	25	25	25	25

Table 4. Quantitative interlobar comparison for magnitude (MAG), high pass filtered phase (PHA), and susceptibility-weighted (SWI) images using nonparametric Friedman test

	MAG	PHA	SWI
P value	0.467	<0.025	0.596
Interlobar comparisons		O vs F ($P < 0.05$) O vs P ($P < 0.05$) P vs F ($P < 0.05$)	

O, occipital lobe; F, frontal lobe; P, parietal lobe; T, temporal lobe

agreement between the qualitative and quantitative results.

SWI is a 3D gradient-echo MR image with high spatial resolution that undergoes phase difference enhancement in postprocessing to produce high contrast between tissues with different susceptibilities.[1] The phase images are high pass filtered and transformed into a phase mask that is later multiplied onto the original MAG image to enhance contrast between tissues with different susceptibilities, resulting in the final SWI.[1] SWI was first developed as a BOLD venography technique[4,22] to demonstrate the difference in local susceptibility between intravascular deoxyhemoglobin and surrounding tissues.[1,20] SWI has also been used to show differences in susceptibility caused by local iron content in the basal ganglia[7] and brain stem.[23] However, SWI has not been used to study interlobar differences of the CMJ that appear as low signal in the subcortical region.

The CMJ is a unique area of the brain known to be rich in iron deposition[24,25] and heavily myelinated.[26] Deposition of non-heme iron will lead to contrast changes in MAG and PHA images. The arcuate segment of the subcortical veins runs in a unique zigzag course in the CMJ to act as a source of deoxyhemoglobin and affect both MAG and PHA images. On the other hand, myelinated arcuate U-fibers in the CMJ lead to contrast changes mainly on the phase images. Using the magnetization transfer ratio as an indirect measure of myelin content in the CMJ, a recent report suggested the variation of myelin as the main source of contrast in the CMJ on phase images.[14] The CMJ appears with low intensity on SWI images, and low signal on SWI comes from either MAG or PHA images. Low signal on MAG images comes from changes induced by local susceptibility to both paramagnetic substances, such as iron, and diamagnetic substances, such as myelin.[1] High signal on PHA images comes mainly from local positive phase caused by iron,[7,11,12,27–29] water-macromolecule exchange,[16,30] anisotropic microscopic tissue architecture, and fiber orientation within the main magnetic field,[31–33] whereas low signal on PHA images comes from local negative phase in response to such diamagnetic substances as myelin. Nevertheless, it has to be noted that diamagnetic substances do not always show low signal on phase images; when considering the relative susceptibilities of substances to water susceptibility, substances less diamagnetic than water (such as lipids) might cause a quasi-paramagnetic effect and show high signal on PHA images.[31] However, very few studies using SWI have involved the CMJ,[14,25] and to the best of our knowledge, there has been no report of the local histological characteristics of interlobar differences in the CMJ.

The only slight agreement between our qualitative and quantitative results can be best explained by differences in the continuity of the CMJ signal between the 2 analyses, fluctuations in signal intensity values, and the conversion of RSR percentages into grades.

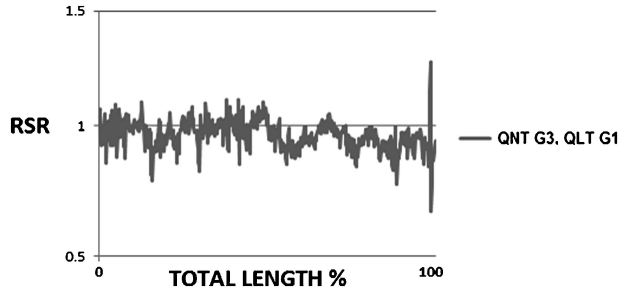

Fig. 2. Quantitative Grade 3 relative signal ratio (RSR) signal profile; the more the sudden fluctuations of RSR value, the more disagreement between the quantitative (QNT) and qualitative (QLT) grades. QNT Grade 3 and QLT Grade 1 had an RSR of 0.75 with many fluctuations.

Continuity of the CMJ signal: By visual qualitative evaluation, we only see the continuous signal of the CMJ (the continuous pixels with low signal on SWI), whereas the quantitative analysis detects all voxels of RSR less than one in SWI and MAG or greater than one in PHA whether or not they are continuous and then converts the total number into grades.

Fluctuations in signal intensity values: The more fluctuations of the RSR, the less agreement between quantitative and qualitative grades because the human eye may be unable to detect RSR values very near to one (no contrast between GM and WM) (Fig. 2).

Conversion of RSR percentages into grades: The results of quantitative analysis are derived as percentages and transformed into grades, each of which covers a range of 25% of the RSR percentage. Qualitatively, many borderline cases might have been graded lower or higher because of the less accurate nature of the visual "subjective" grading. PHA images are most sensitive to phase variation in local susceptibility and would show better contrast between the CMJ and neighboring WM. MAG images are not as sensitive as PHA images for the local substance variations mentioned and therefore not as sensitive as PHA in distinguishing the CMJ from neighboring WM. Though SWI combines the 2 images, contrast from the MAG image might obscure the contrast between the CMJ and WM from the PHA image in some areas at the voxel level. Therefore, quantitative analysis of SWI, its underlying PHA, and MAG images would reveal any subtle changes in signal intensity that qualitative analysis alone does not permit.

The CMJ is rich in iron,[12,24,25] and its iron content is higher than that of the underlying white matter,[24,27,34] so iron rather than myelin may be the source of the low signal of the CMJ on SWI. However, this is beyond the scope of our study and requires more advanced postprocessing methods, such as quantitative susceptibility mapping, to investigate further the cause of local susceptibility at the CMJ. The OR, on the other hand, is rich in myelin and low in iron content and appears as a low signal (diamagnetic) on PHA images compared to the high signal of the CMJ (paramagnetic).[10,31,34] A reported difference in interhemispheric and interlobar iron concentration[35,36] might give clues to the interlobar difference in the appearance of the CMJ in our results.

Our study is limited because we evaluated only patients with preoperative brain tumor. A larger study sample is needed to study further age-related changes in CMJ appearance, and more sophisticated post-processing tools are needed to investigate further the causes of interlobar differences. We also did not perform region-specific analysis (in areas known to have high iron content, such as the motor cortex) within the different lobes to investigate intralobar differences in the CMJ signal.

Conclusion

Qualitatively, the appearance of the CMJ differed significantly among the different lobes of the brain on SWI and underlying PHA images but not on MAG images. Quantitatively, only PHA images showed a significant interlobar difference of RSR. PHA images are most sensitive to CMJ signal contrast due to local paramagnetic iron content.

Acknowledgement

We are grateful to Dr. Yukio Miki for his guidance and continuous help throughout this research. This work was supported in part by a Japanese Ministry of Education, Culture, Sports, Science, and Technology grant-in-aid for scientific research, (B) (21390344).

References

1. Haacke EM, Xu Y, Cheng YC, Reichenbach JR. Susceptibility weighted imaging (SWI). Magn Reson Med 2004; 52:612–618.
2. Wycliffe ND, Choe J, Holshouser B, Oyoyo UE, Haacke EM, Kido DK. Reliability in detection of hemorrhage in acute stroke by a new three-dimensional gradient recalled echo susceptibility-weighted imaging technique compared to computed tomography: a retrospective study. J Magn Reson Imaging 2004; 20:372–377.
3. Shimoda Y, Kudo K, Kuroda S, et al. Susceptibility-

weighted imaging and magnetic resonance angiography during migraine attack: a case report. Magn Reson Med Sci 2011; 10:49–52.
4. Reichenbach JR, Barth M, Haacke EM, Klarhöfer M, Kaiser WA, Moser E. High-resolution MR venography at 3.0 Tesla. J Comput Assist Tomogr 2000; 24: 949–957.
5. Suzuki M, Kudo K, Sasaki M, et al. Detection of active plaques in multiple sclerosis using susceptibility-weighted imaging: comparison with gadolinium-enhanced MR imaging. Magn Reson Med Sci 2011; 10:185–192.
6. Yao B, Li TQ, Gelderen Pv, Shmueli K, de Zwart JA, Duyn JH. Susceptibility contrast in high field MRI of human brain as a function of tissue iron content. Neuroimage 2009; 44:1259–1266.
7. Haacke EM, Miao Y, Liu M, et al. Correlation of putative iron content as represented by changes in R2* and phase with age in deep gray matter of healthy adults. J Magn Reson Imaging 2010; 32: 561–576.
8. Ochi T, Taoka T, Akashi T, et al. Discrepancy in T_1 and T_2 shortening of the globus pallidus in hepatic insufficiency: evaluation by susceptibility-weighted imaging. Magn Reson Med Sci 2011; 10:79–83.
9. Wu Z, Mittal S, Kish K, Yu Y, Hu J, Haacke EM. Identification of calcification with MRI using susceptibility-weighted imaging: a case study. J Magn Reson Imaging 2009; 29:177–182.
10. Mori N, Miki Y, Kasahara S, et al. Susceptibility-weighted imaging at 3 Tesla delineates the optic radiation. Invest Radiol 2009; 44:140–145.
11. Duyn JH, van Gelderen P, Li TQ, de Zwart JA, Koretsky AP, Fukunaga M. High-field MRI of brain cortical substructure based on signal phase. Proc Natl Acad Sci USA 2007; 104:11796–11801.
12. Lee J, Hirano Y, Fukunaga M, Silva AC, Duyn JH. On the contribution of deoxy-hemoglobin to MRI gray-white matter phase contrast at high field. Neuroimage 2010; 49:193–198.
13. Haacke EM, Cheng NY, House MJ, et al. Imaging iron stores in the brain using magnetic resonance imaging. Magn Reson Imaging 2005; 23:1–25.
14. Langkammer C, Krebs N, Goessler W, et al. Susceptibility induced gray-white matter MRI contrast in the human brain. Neuroimage 2012; 59:1413–1419.
15. Liu C, Li W, Johnson GA, Wu B. High-field (9.4 T) MRI of brain dysmyelination by quantitative mapping of magnetic susceptibility. Neuroimage 2011; 56:930–938.
16. Zhong K, Leupold J, von Elverfeldt D, Speck O. The molecular basis for gray and white matter contrast in phase imaging. Neuroimage 2008; 40:1561–1566.
17. Nakada T, Matsuzawa H, Igarashi H, Kwee IL. Expansion of corticomedullary junction high-susceptibility region (CMJ-HSR) with aging: a clue in the pathogenesis of Alzheimer's disease? J Neuroimaging 2012; 22:379–383.
18. Yoshiura T, Mihara F, Koga H, et al. Mapping of subcortical white matter abnormality in Alzheimer's disease using diffusion-weighted magnetic resonance imaging. Acad Radiol 2006; 13:1460–1464.
19. Mehemed TM, Yamamoto A. High-pass-filtered phase image: left- versus right-handed MR imaging systems. AJNR Am J Neuroradiol 2013; 34:E72.
20. Haacke EM, Mittal S, Wu Z, Neelavalli J, Cheng YC. Susceptibility-weighted imaging: technical aspects and clinical applications, part 1. AJNR Am J Neuroradiol 2009; 30:19–30.
21. Schneider CA, Rasband WS, Eliceiri KW. NIH Image to ImageJ: 25 years of image analysis. Nat Methods 2012; 9:671–675.
22. Reichenbach JR, Essig M, Haacke EM, et al. High-resolution venography of the brain using magnetic resonance imaging. MAGMA 1998; 6:62–69.
23. Manova ES, Habib CA, Boikov AS, et al. Characterizing the mesencephalon using susceptibility-weighted imaging. AJNR Am J Neuroradiol 2009; 30:569–574.
24. Drayer B, Burger P, Darwin R, Riederer S, Herfkens R, Johnson GA. MRI of brain iron. AJR Am J Roentgenol 1986; 147:103–110.
25. Abduljalil AM, Schmalbrock P, Novak V, Chakeres DW. Enhanced gray and white matter contrast of phase susceptibility-weighted images in ultra-high-field magnetic resonance imaging. J Magn Reson Imaging 2003; 18:284–290.
26. Ashikaga R, Araki Y, Ono Y, Nishimura Y, Ishida O. Appearance of normal brain maturation on fluid-attenuated inversion-recovery (FLAIR) MR images. AJNR Am J Neuroradiol 1999; 20:427–431.
27. Bagnato F, Hametner S, Yao B, et al. Tracking iron in multiple sclerosis: a combined imaging and histopathological study at 7 Tesla. Brain 2011; 134:3602–3615.
28. Hopp K, Popescu BF, McCrea RP, et al. Brain iron detected by SWI high pass filtered phase calibrated with synchrotron X-ray fluorescence. J Magn Reson Imaging 2010; 31:1346–1354.
29. Fukunaga M, Li TQ, van Gelderen P, et al. Layer-specific variation of iron content in cerebral cortex as a source of MRI contrast. Proc Natl Acad Sci USA 2010; 107:3834–3839.
30. Shmueli K, Dodd SJ, Li TQ, Duyn JH. The contribution of chemical exchange to MRI frequency shifts in brain tissue. Magn Reson Med 2011; 65:35–43.
31. He X, Yablonskiy DA. Biophysical mechanisms of phase contrast in gradient echo MRI. Proc Natl Acad Sci USA 2009; 106:13558–13563.
32. Lee J, Shmueli K, Fukunaga M, et al. Sensitivity of MRI resonance frequency to the orientation of brain tissue microstructure. Proc Natl Acad Sci USA 2010; 107:5130–5135.
33. Lee J, van Gelderen P, Kuo LW, Merkle H, Silva AC, Duyn JH. T_2*-based fiber orientation mapping. Neuroimage 2011; 57:225–234.
34. Curnes JT, Burger PC, Djang WT, Boyko OB. MR imaging of compact white matter pathways. AJNR

Am J Neuroradiol 1988; 9:1061–1068.
35. Hallgren B, Sourander P. The effect of age on the non-haemin iron in the human brain. J Neurochem 1958; 3:41–51.
36. Xu X, Wang Q, Zhang M. Age, gender, and hemispheric differences in iron deposition in the human brain: an *in vivo* MRI study. Neuroimage 2008; 40: 35–42.